Article

Optical Detection of Underwater Propeller Wake Based on a Position-Sensitive Detector

Guanlong Zhou [1,2], Qin Liu [2], Hu Wang [2], Liyan Li [2,*], Yan Zhou [2] and Xinyu Chen [1,*]

1 School of Physics, Changchun University of Science and Technology, Changchun 130022, China; zhouguanlong0104@163.com

2 Optoelectronics System Laboratory, Institute of Semiconductors, Chinese Academy of Sciences, Beijing 100083, China; liuqin@semi.ac.cn (Q.L.); wanghu@semi.ac.cn (H.W.); zhouyan@semi.ac.cn (Y.Z.)

* Correspondence: lyli@semi.ac.cn (L.L.); chenxinyucust@163.com (X.C.)

Abstract: The study of underwater vehicle wake detection is of significant importance within the field of target detection, localisation, and tracking of underwater vehicles. Given that propellers are the propellers of modern ships and underwater vehicles, the propeller wake field represents the principal target source for wake detection in underwater vehicles. The objective of this paper is to propose a method for measuring the wake of an underwater propeller based on a position-sensitive detector. A theoretical model of the relationship between the laser spot displacement and the change in the refractive index of the wake field is established on the basis of the principle of laser beam deflection. A prototype experimental setup for underwater propeller wake measurement was constructed based on the aforementioned optical measurement method. Furthermore, the simulation of the propeller wake flow field with strong density stratification and linear density stratification was conducted based on the experimental setup. Furthermore, experiments were conducted to detect the flow field of a propeller wake. The experimental results indicate that the wake dissipation times of the propeller in a strong density-stratified water environment are approximately 800 s and 750 s. Following the stabilisation of the wake field density, the laser spot position is observed to be stable at 0.341 mm and 0.441 mm, respectively, with a corresponding refractive index change of 2.99×10^{-6} RIU (refractive index unit) and 3.87×10^{-6} RIU, respectively. These experimental results are found to be in general agreement with the simulation results of the propeller wake field. A comparison of the experimental wake measurements based on the device with the wake measurements based on a CTD (conductivity–temperature–depth) device reveals a consistent trend. The realisation of this detection technique is of great significance for the advancement of research in the field of optical detection of underwater vehicle wake streams.

Keywords: underwater propeller wake; position-sensitive detector; optical detection

1. Introduction

The study of underwater vehicle wake detection is of significant importance within the field of target detection, localisation, and tracking of underwater vehicles [1]. For an extended period, traditional acoustic detection technology has been the primary method employed to detect underwater vehicles [2,3]. Nevertheless, the advancement of noise reduction technology for underwater vehicles has resulted in a significant reduction in the self-noise of these vehicles, which is now nearly indistinguishable from the background noise of the ocean [4–6]. Consequently, traditional sonar equipment is no longer capable of detecting underwater vehicles. This indicates the necessity for alternative methods of underwater vehicle detection to overcome the limitations of acoustic detection by underwater vehicles. In order to enhance the efficacy of underwater vehicle detection, non-acoustic detection technology has increasingly become a focal point of investigation.

Among the numerous non-acoustic methodologies for the detection of submerged vehicles, there are some promising non-acoustic techniques such as magnetic anomaly

detection [7], LIDAR [8,9], and bioluminescence detection [10] for the same purpose, but they have some inherent limitations, such as low detection accuracy, a narrow detection range, and a high degree of environmental influence, which restrict their use for detection over a wide area and from a large distance [11]. The flow field generated by an underwater vehicle can serve as a valuable source of information for the development of underwater vehicle detection techniques, given its prolonged duration and extensive extension distance in density-stratified fluids [12–14]. Biologists have discovered that marine animals possess the most well-documented underwater wake detection system, with fin-footed animals such as seals, sea lions, and walruses demonstrating the capacity to detect underwater propagating disturbances through their facial antennae [15–17]. In 1998, Dehnhardt G et al. employed a trained seal to investigate the capacity to detect minute underwater disturbances in the absence of any non-contact sensory cues. This study revealed that a minimum fluid velocity of 245 μm/s could be detected in the range of 10–100 Hz [18]. In 2016, Eberhardt, WC et al. proposed a bionic detection system based on underwater vehicle wake characteristics based on the capacitive inductive principle [19]. It was found that the bionic whiskers can give signals of the travelling path direction of the underwater vehicle model, but the tracking trajectory has some deviations. In 1880, Dvorak initially proposed an optical system that was deemed suitable for observing changes in fluid density flow. The fundamental principle is that the point light source is collimated through the wake field, which is a consequence of the fluid density gradient changes. This results in the deflection of the collimated light, which in turn gives rise to spatial variations in light intensity, with bright and dark areas on the screen [11]. In 2000, Dalziel SB et al. employed a line-mode synthetic rippling method utilising digital recording to generate a virtual mask in front of a camera, thereby enabling the measurement of the density gradient variation of the flow field in the wake of an underwater vehicle [20]. In 2004, Elsinga GE et al. used a standard Z-type parabolic mirror rippler to make quantitative measurements of the flow field [21]. In 2012, Hargather MJ et al. incorporated calibration means and data analysis and processing software into a detection method based on that employed by Elsinga GE. The resulting experiments demonstrated that the sensitivity for detecting refractive indices induced by underwater vehicles was 10^{-5} RIU [22]. In 2016, Ben-Gida H et al. performed wake field imaging detection experiments on an underwater vehicle model using particle image velocimetry (PIV) [23]. In 2000, Stella A et al. used laser Doppler velocimetry (LDV) to probe the wake field of an underwater vehicle propeller model [24]. In 2017, Paik, BG et al. conducted cavitation tests on the propeller of an underwater vehicle using LDV in a large vacuolar water cylinder at KRISO. The test results demonstrated a high degree of correlation between the measured propeller wake and the CFD calculations [25]. In 2013, Tatavarti R. et al. constructed an underwater vehicle wake flow field detection system based on the principle of laser deflection. This was mounted on an oceanographic research vessel and placed at a depth of 42 m underwater, with the aim of monitoring the A74 ocean acoustic research vessel. The system was successfully employed to detect the flow field in its wake, and the detection system had a sensitivity of 10^{-6} RIU for refractive index detection due to wake turbulence [26].

Nevertheless, the shading technique is only capable of establishing the presence or absence of a wake flow, yet it is unable to ascertain the direction of light deflection and sensitivity is low [11]. The density gradient of the wake stream can be known by the shadow detection technique, and the detection sensitivity of the shadow system is limited by the amount of knife cut due to the blockage of the cutter to determine the direction of vertical movement of the light. Particle image velocimetry relies on tracer particles and is therefore only suitable for small-area system detection. Laser Doppler velocimetry has a large deviation in wake detection because of the signal drift during the long detection time [27]. In the laser deflection detection technique, the output current of the photodiode is processed by the beam position and power measurement system, so as to obtain the change in laser intensity and deflection related to the nature of the medium wake field; the corresponding detection system has been applied to test experiments, and

has successfully detected the detection target at 8 km through the wake current [26]. A comparative analysis of non-acoustic detection methods reveals that the laser deflection principle exhibits superior sensitivity and stability in the detection of underwater vehicle wakes.

In light of the necessity for an underwater vehicle wake detection method that is capable of accurately identifying the position of the vehicle in question, we propose a position-sensitive detector-based approach that utilises the laser deflection principle. A theoretical model was developed which describes the relationship between the displacement of a laser spot and the gradient change in the refractive index in the wake field of an underwater vehicle. This model was based on the principle of laser beam deflection. Based on this optical detection method, an experimental apparatus for the detection of the wake current field of underwater vehicles was constructed. Since propellers are the propellers of modern ships and underwater vehicles [28–30], propellers were chosen as the power source of the target wake flow. In the design of the experimental setup, a three-bladed propeller with a diameter of 39 mm was selected, the water tank size was 980 mm × 380 mm × 380 mm, and the laser acted at a distance of 550 mm from the propeller. The sensitivity of the refractive index gradient measurement of the wake field based on the parameters of this propeller wake measurement device was calculated to be 8.77×10^{-9} RIU. The experimental results show that in a strong density-stratified water environment, the detection signal of the propeller wake field persisted for approximately 800 s. As the wake field power attenuated continuously, the wake field density gradually stabilises, with the final laser spot position stabilising at 0.341 mm. This corresponded to a change in the refractive index of the flow field of 2.99×10^{-6} RIU. In a linear density-stratified water environment, the detection signal of the propeller wake field lasted approximately 750 s. As the wake field power was attenuated continuously, the wake field density gradually stabilised, with the final laser spot position stabilising at 0.441 mm. This corresponded to a change in the refractive index of the flow field of 3.87×10^{-6} RIU. The signal characteristics of the propeller wake field, as measured by the PSD-based experimental setup for underwater propeller wake measurement, were found to be essentially consistent with those of the corresponding simulation results. A comparison of the experimental device-based wake measurements with the CTD-based wake measurements revealed a consistent trend.

2. Principle of the Underwater Vehicle Wake Detection

The principle underlying underwater vehicle wake detection is that of laser beam deflection, as illustrated in the schematic diagram presented in Figure 1. The laser beam is incident vertically upon the glass water cylinder, subsequently reaching the designated area for the detection of underwater vehicle wakes. The propeller disturbance caused by the refractive index gradient change for the wake field results in a laser and wake field interaction, which is manifested as a deflection phenomenon. Subsequently, the laser traverses the glass water cylinder and is focused to a point on the photosensitive surface of the PSD via a focusing lens. Consequently, the position coordinates of the laser spot following the perturbation of the wake field are obtained utilising the PSD.

In light of the existence of a refractive index gradient in the y, z direction of the flow field, it can be expressed as follows [10]:

$$\frac{\partial^2 y}{\partial x^2} = \frac{1}{n}\frac{\partial n}{\partial y} \tag{1}$$

$$\frac{\partial^2 z}{\partial x^2} = \frac{1}{n}\frac{\partial n}{\partial z} \tag{2}$$

where x is the direction of light propagation, n is the refractive index, and the curvatures of the refracted light $\frac{\partial^2 y}{\partial x^2}$ and $\frac{\partial^2 z}{\partial x^2}$ are represented by the gradients of the refractive index $\frac{\partial n}{\partial y}$ and $\frac{\partial n}{\partial z}$ of the underwater vehicle wake.
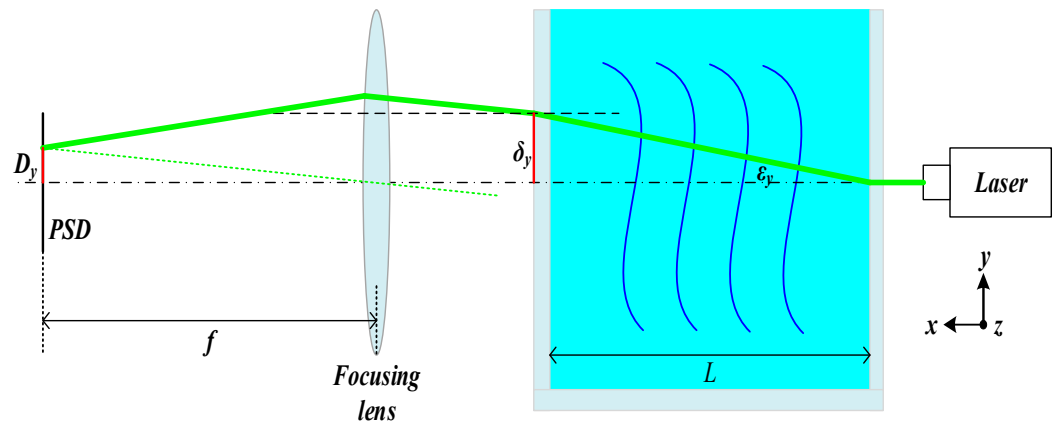
Figure 1. Schematic diagram of underwater vehicle wake detection based on the laser beam deviation technique.

In the underwater vehicle wake current field detection area, the angle of deflection of the light ray in the direction of the y and z axes is obtained by integrating Equations (1) and (2), as follows:

$$\varepsilon_y = \frac{1}{n} \int \frac{\partial n}{\partial y} \partial x \tag{3}$$

$$\varepsilon_z = \frac{1}{n} \int \frac{\partial n}{\partial z} \partial x \tag{4}$$

where ε_y is the angle of deflection of the light ray in the direction of y axis and $\frac{\partial n}{\partial y}$ is the gradient of the refractive index in the y axis direction, whereas ε_z is the angle of deflection of the light ray in the direction of z axis and $\frac{\partial n}{\partial z}$ is the gradient of the refractive index in the z axis direction.

Since the deflection angle is small and the distance of the laser through the flow field is L, there is the following relationship:

$$\varepsilon_y = \frac{L}{n_0} \frac{\partial n}{\partial y} \approx \tan \varepsilon_y \tag{5}$$

$$\varepsilon_z = \frac{L}{n_0} \frac{\partial n}{\partial z} \approx \tan \varepsilon_z \tag{6}$$

where n_0 is the refractive index of the underwater vehicle wake field before perturbation.

Therefore, the gradient of the refractive index in the y axis direction is expressed as follows:

$$\frac{\partial n}{\partial y} = \tan \varepsilon_y \frac{n_0}{L} = \frac{\delta_y n_0}{L^2} \tag{7}$$

The same reasoning can be applied:

$$\frac{\partial n}{\partial z} = \tan \varepsilon_z \frac{n_0}{L} = \frac{\delta_z n_0}{L^2} \tag{8}$$

where δ_y is the displacement of the light ray in the direction of the y axis, and δ_z is the displacement of the light ray in the direction of the z axis.

Refraction occurs when the laser light passes from the flow field through the glass on the wall of the water tank, which satisfies the law of refraction, so the refractive index gradient with respect to positions D_y and D_z on the photosensitive surface of the PSD is expressed as:

$$\frac{\partial n}{\partial y} = \frac{D_y}{f L} \tag{9}$$

$$\frac{\partial n}{\partial z} = \frac{D_z}{fL} \tag{10}$$

where f is the focal length of the focusing lens.

3. Experimental Setup

The propeller wake detection experimental setup is shown in Figure 2. A three-bladed propeller with a diameter of 39 mm was selected for the experiment, and the structure of the propeller is illustrated in Figure 2a. And the propeller speed is 110 revolutions per second. The configuration of the experimental setup for propeller wake detection is illustrated in Figure 2b.
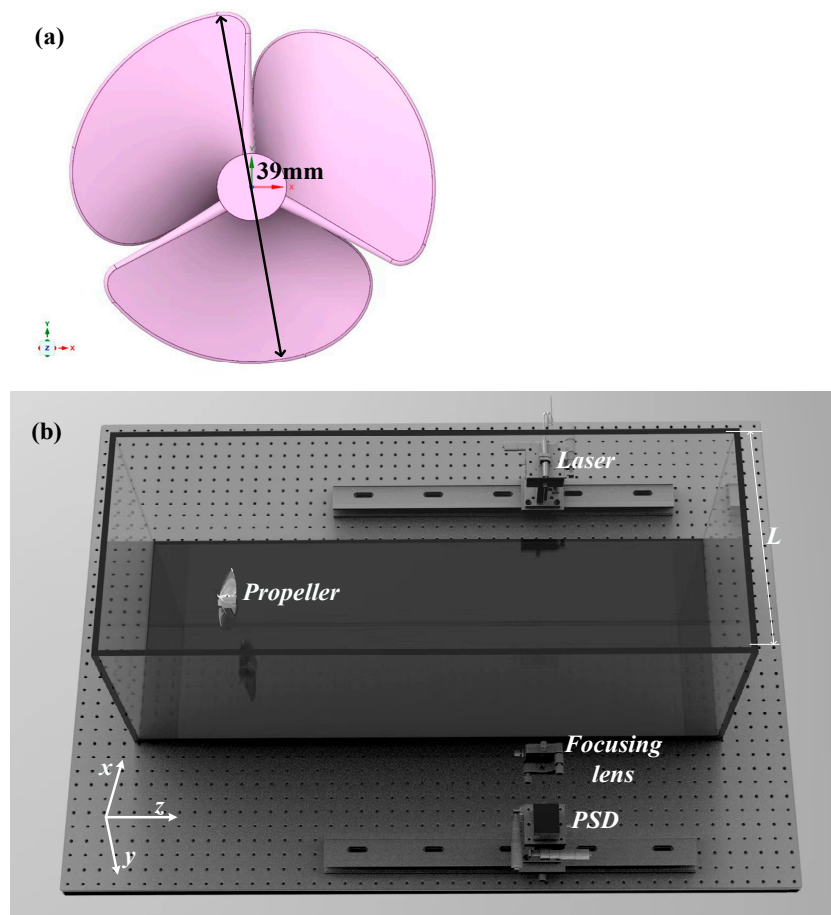

Figure 2. The propeller wake detection experimental setup. (**a**) The structure of the three-bladed propeller; (**b**) the configuration of the experimental setup for propeller wake detection.

In the experiment, in order to reduce the impact of the propeller wake field on the glass water tank wall, a 980 mm × 380 mm × 380 mm glass water tank was selected for flow field detection experiments, the glass water tank wall flatness was good, and the laser incident and outgoing wake field of the two glass walls was parallel to each other. The propeller was positioned at a distance of 115 mm from the bottom surface of the glass tank and 150 mm from the left wall surface of the glass tank, with the centre of the propeller located at this point. In order to minimise the absorption and scattering effects of seawater on the detection light source, a green collimated laser with a centre wavelength of 532 nm was employed as the detection light source in the wake field detection device. The laser beam was directed vertically into the wake field at a distance of 500 mm from the propeller, at the same height as the centre of the propeller. After interacting with the propeller wake field, the laser was focused onto the PSD photosensitive surface using a lens with a focal

length of 300 mm. The dimensions of the PSD's photosensitive area were 4 mm × 4 mm, and the position measurement resolution was approximately 1 μm. To ensure the positional resolution of the PSD in front of the light-sensitive surface of the PSD, a narrow-band light filter, with the same peak wavelength and a bandwidth of 0.9 nm, was used to filter out the stray light, except for the 532 nm measurement light. And it is imperative that the PSD photosensitive surface remains parallel to the laser outgoing surface of the glass water tank. The sensitivity of the refractive index gradient measurement of the wake field based on the parameters of this propeller wake measurement device was calculated to be 8.77×10^{-9} RIU according to theoretical Equations (9) and (10).

4. Simulation Analysis

The propeller wake was simulated and analysed based on the propeller wake measurement experimental setup described above. The centre of the propeller was taken as the symmetry axis, and two cross sections in different directions, transverse (xz-plane) and longitudinal (yz-plane), were selected for the purpose of analysing the spatial evolution law of the propeller wake flow field.

The results of the propeller wake simulation at strong density stratification are shown in Figure 3. During the wake field simulation, a water depth of 230 mm was set, and the depth of 115 mm represented a strong density-stratified interface, which was consistent with the height of the propeller centre. The upper layer was composed of pure water with a density of 1000 kg/m^3, while the lower layer was seawater with a salinity of approximately 20 PSU and a density of 1014 kg/m^3. The relationship between the refractive index and the density of a propeller wake was given by the Gladstone–Dale equation, $n = 1 + \kappa\rho$, where n is the optical refractive index, ρ the density of the fluid, and κ is a constant coefficient which is a function of the laser wavelength and the fluid characteristics [26]. This is indicative of a refractive index of approximately 1.34 RIU for the upper layer of pure water and 1.34476 RIU for the lower layer of brine. The optical refractive index was linearly related to fluid density. Figure 3a illustrates the density distribution of the wake field in the yz-plane following 0.2 s of propeller rotation. The wake was propelled to a distance of 380 mm from the propeller, with the density within the wake field ranging from 1002 kg/m^3 to 1011 kg/m^3. The corresponding refractive indices were approximately 1.34068 RIU to 1.34374 RIU. Figure 3b illustrates the density distribution of the wake field in the xz-plane following 0.2 s of propeller rotation. The density within the wake field was observed to range from 1008 kg/m^3 to 1010 kg/m^3. The corresponding refractive indices were approximately 1.34272 RIU to 1.3434 RIU. The propeller rotated for 5 s and then stopped rotating. Figure 3c,d illustrate the density distributions of the wake field in the yz and xz-plane, respectively, following a 5.4 s rotation of the propeller. The density within the wake field ranged from 1011 kg/m^3 to 1013 kg/m^3. The corresponding refractive indices were approximately 1.34374 RIU to 1.34442 RIU. Figure 3e,f show the density distributions of the wake field in the yz and xz-plane, respectively, after the propeller rotated for 15.4 s. The density within the wake field ranged from 1011 kg/m^3 to 1012 kg/m^3. The corresponding refractive indices were approximately 1.34374 RIU to 1.34408 RIU. The simulation of the propeller wake field in the case of strong density stratification revealed that when the propeller stopped rotating, the density distribution range of the wake field gradually became smaller. This indicated that the density of the propeller wake field was gradually becoming uniform and stable.

The results of the propeller wake simulation under conditions of linear density stratification are presented in Figure 4. During the wake field simulation, a water depth of 230 mm was set, and the density distribution varied linearly with depth. The density of the top water layer was 1001 kg/m^3 and the density of the bottom water layer was 1014 kg/m^3. The corresponding refractive index of the top water layer was 1.34034 RIU and the refractive index of the bottom water layer was 1.34476 RIU. Figure 4a illustrates the density distribution of the wake field in the yz-plane following 0.2 s of propeller rotation. The wake was propelled to a distance of 380 mm from the propeller, with the density within the wake

field ranging from 1004 kg/m³ to 1009 kg/m³. The corresponding refractive indices were approximately 1.34136 RIU to 1.34306 RIU. Figure 4b illustrates the density distribution of the wake field in the *xz*-plane following 0.2 s of propeller rotation. The density within the wake field was observed to range from 1007 kg/m³ to 1009 kg/m³. The corresponding refractive indices were approximately 1.34238 RIU to 1.34306 RIU. The propeller rotated for 5 s and then stopped rotating. Figure 4c,d illustrate the density distributions of the wake field in the *yz*- and *xz*-plane, respectively, following a 5.4 s rotation of the propeller. The density within the wake field ranged from 1011 kg/m³ to 1013 kg/m³. The corresponding refractive indices were approximately 1.343374 RIU to 1.34442 RIU. Figure 4e,f show the density distributions of the wake field in the *yz*- and *xz*-plane, respectively, after the propeller rotated for 15.4 s. The density within the wake field ranged from 1012 kg/m³ to 1013 kg/m³. The corresponding refractive indices were approximately 1.34408 RIU to 1.34442 RIU. The simulation of the propeller wake field in the case of linear density stratification revealed that when the propeller stopped rotating, the density distribution range of the wake field gradually became smaller. This indicated that the density of the propeller wake field was gradually becoming uniform and stable.

In comparison to the strong density stratification case, the density distribution range of the propeller wake field was 4 kg/m³ smaller in the linear density case when the propeller was rotating. However, when the density tended to be uniform and stable, the density range of the wake field remained largely unchanged.
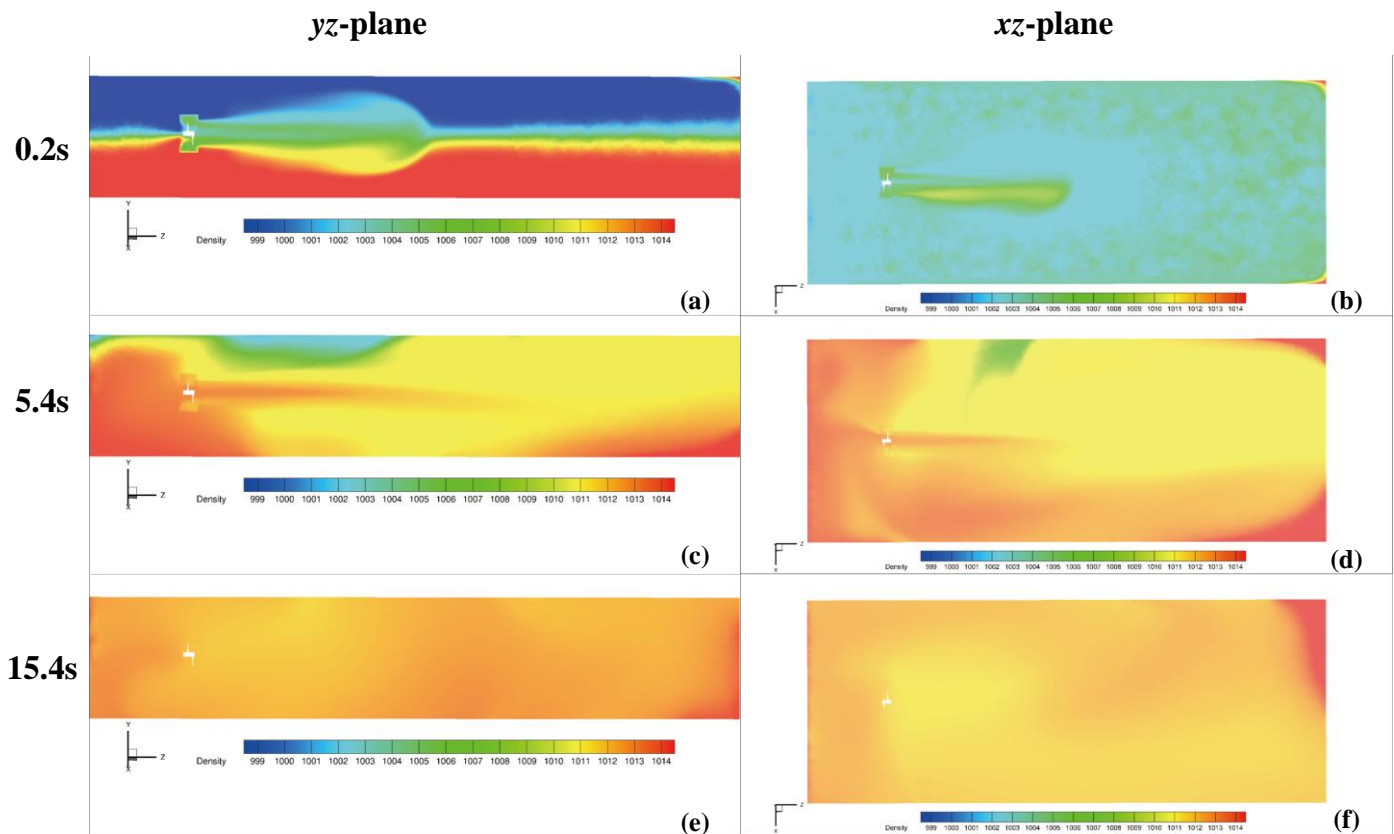

Figure 3. The simulation results of propeller wake at strong density stratification. (**a**) The density distribution of the wake field in the *yz*-plane following 0.2 s of propeller rotation; (**b**) the density distribution of the wake field in the *xz*-plane following 0.2 s of propeller rotation; (**c**) the density distribution of the wake field in the *yz*-plane following 5.4 s of propeller rotation; (**d**) the density distribution of the wake field in the *xz*-plane following 5.4 s of propeller rotation; (**e**) the density distribution of the wake field in the *yz*-plane following 15.4 s of propeller rotation; (**f**) the density distribution of the wake field in the *xz*-plane following 15.4 s of propeller rotation.
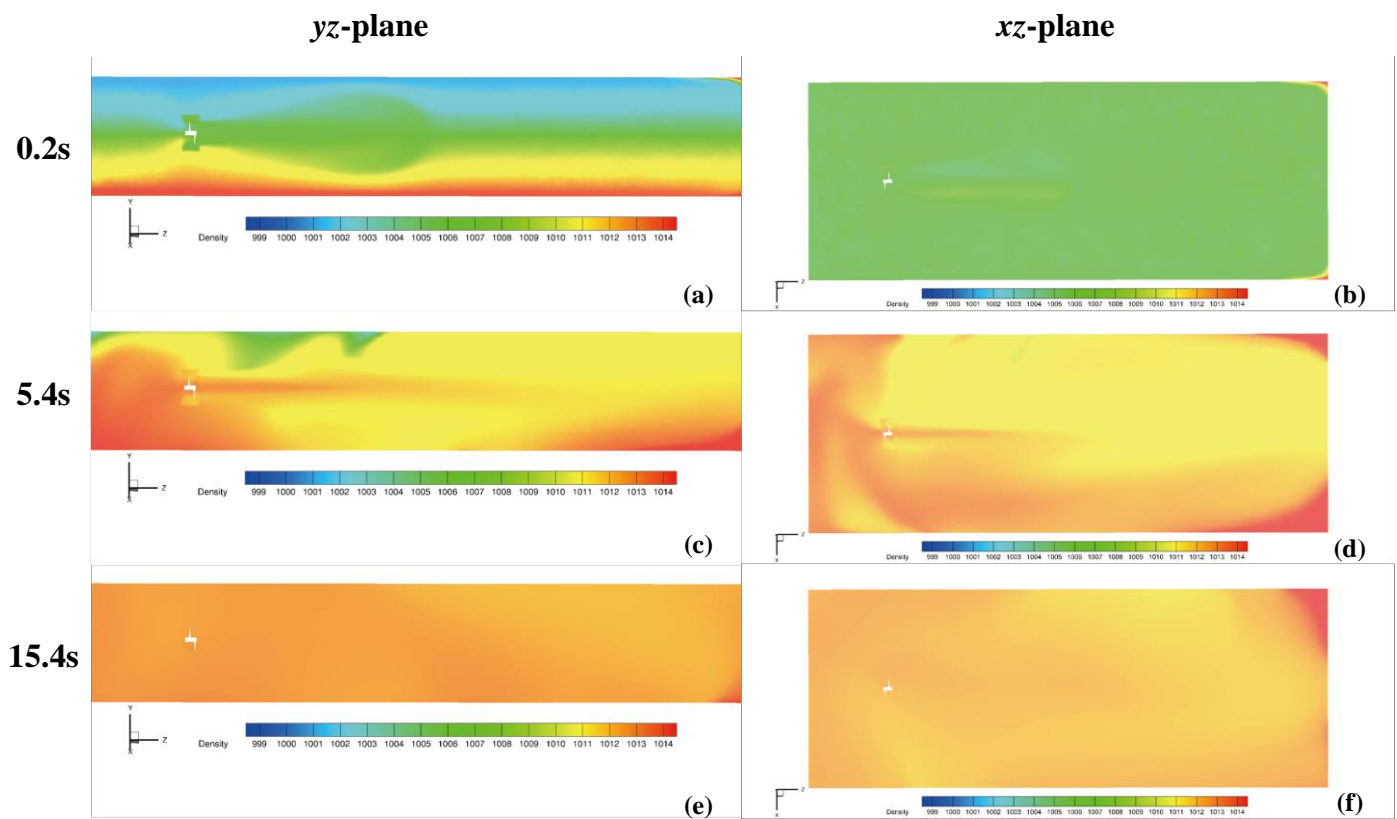
yz-plane　　　　　　　　　　　　　　　　**xz-plane**

Figure 4. The simulation results of the propeller wake under linear density stratification conditions. (**a**) The density distribution of the wake field in the *yz*-plane following 0.2 s of propeller rotation; (**b**) the density distribution of the wake field in the *xz*-plane following 0.2 s of propeller rotation; (**c**) the density distribution of the wake field in the *yz*-plane following 5.4 s of propeller rotation; (**d**) the density distribution of the wake field in the *xz*-plane following 5.4 s of propeller rotation; (**e**) the density distribution of the wake field in the *yz*-plane following 15.4 s of propeller rotation; (**f**) the density distribution of the wake field in the *xz*-plane following 15.4 s of propeller rotation.

5. Results and Discussion

5.1. Results of Propeller Wake Measurements Conducted in a Strong Density Stratification Water Environment

In the experiment, the propeller was fixed in a strongly density-stratified water environment, with the centre of the propeller maintained at the same height as the strongly density-stratified interface. Conductivity measurements were taken using a CTD (conductivity–temperature–depth) to determine the conductivity change in the water environment at different underwater depths, and the resulting density profiles were calculated. The resulting density change curve with depth change is shown in Figure 5. The upper water layer had a density of approximately 1000 kg/m^3, while the lower salted water layer had a density of approximately 1014 kg/m^3. The corresponding refractive index of the top water layer was approximately 1.34 RIU and the refractive index of the bottom water layer was approximately 1.34476 RIU.

The sampling frequency of the experimental setup was set to 10 kHz, and prior to the collection of laser spot position data, it was necessary to calibrate the laser spot position to the zero point of the PSD photosensitive surface. The results of propeller wake measurements conducted in a strong density stratification water environment are presented in Figure 6a. The ambient signal was acquired for a period of 60 s prior to the commencement of propeller rotation. The propeller rotated at a rate of 110 revolutions per second for a period of 5 s, after which it ceased to rotate. A total of 1800 s of signals were acquired for the experiment. Following the cessation of propeller rotation, the laser

spot position underwent a significant change for approximately 360 s. The maximum displacement of the laser spot was 4.689 mm. As the wake field dynamics decreased, the wake density stabilised after 800 ds following the cessation of propeller rotation and the position of the laser spot remained constant. The position of the laser spot was stabilised at 0.341 mm. The sensitivity of the propeller wake measurement device in terms of refractive index measurement was taken into account, and this displacement corresponded to a refractive index change of 2.99×10^{-6} RIU caused by the propeller wake flow field in the detection zone. The laser spot position signal generated by the propeller wake exhibited a decreasing amplitude over time. This phenomenon could be observed as the laser spot displacement gradually diminished as the propeller wake dissipated. Figure 6b illustrates the background position signal, the laser position signal induced by 5 s of propeller rotation, and the laser position signal 25 s after the propeller stops rotating. These signals were measured in the propeller wake for a strongly stratified water environment. The alteration in the laser position signal resulting from the propeller wake was largely in accordance with the simulation outcomes pertaining to the wake field. Figure 6c illustrates the density signal generated by the propeller wake flow, as obtained through CTD measurement. The trend in the density change in the wake field was found to be essentially concordant with the trend in the wake measurement results obtained by means of a PSD-based propeller wake measurement device.
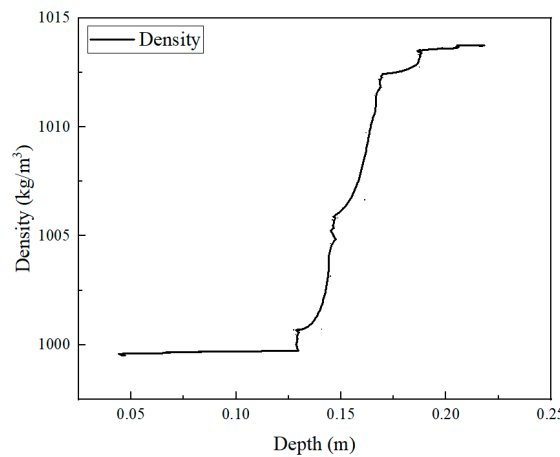

Figure 5. The resulting density change curve with depth change in a strongly density-stratified water environment.
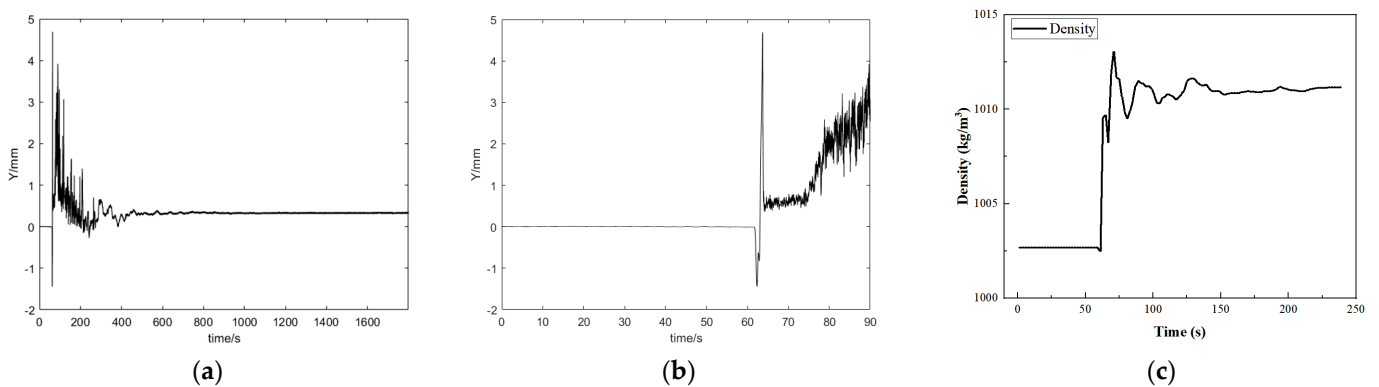

(a) **(b)** **(c)**

Figure 6. (**a**) The results of propeller wake measurements based on a PSD conducted in a strong density stratification water environment; (**b**) the first 90 s of the results of propeller wake measurements based on a PSD conducted in a strong density stratification water environment; (**c**) the results of propeller wake measurements based on a CTD conducted in a strong density stratification water environment.

5.2. Results of Propeller Wake Measurements Conducted in a Linear Density Stratification Water Environment

In the experiment, the propeller was fixed in a linear density-stratified water environment. Conductivity measurements were taken using a CTD to determine the conductivity change in the water environment at different underwater depths, and the resulting density profiles were calculated. The resulting density change curve with depth change is shown in Figure 7. The upper water layer had a density of approximately 1009.5 kg/m^3, while the lower salted water layer had a density of approximately 1013.4 kg/m^3. The corresponding refractive index of the top water layer was approximately 1.34323 RIU and the refractive index of the bottom water layer was approximately 1.344556 RIU. The density varied linearly with depth underwater.
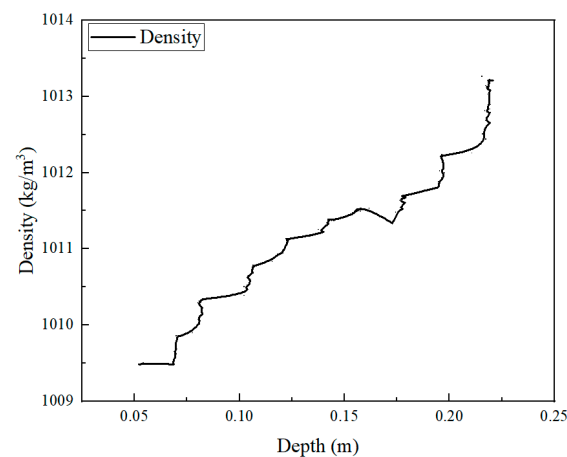

Figure 7. The resulting density change curve with depth change in a linear density-stratified water environment.

The sampling frequency of the experimental setup was set to 10 kHz, and prior to the collection of laser spot position data, it was necessary to calibrate the laser spot position to the zero point of the PSD photosensitive surface. The results of propeller wake measurements conducted in a linear density stratification water environment are presented in Figure 8a. The ambient signal was acquired for a period of 60 s prior to the commencement of propeller rotation. The propeller rotated at a rate of 110 revolutions per second for a period of 5 s, after which it ceased to rotate. A total of 1800 s of signals were acquired for the experiment. Following the cessation of propeller rotation, the laser spot position underwent a significant change for approximately 240 s. The maximum displacement of the laser spot was 1.673 mm. As the wake field dynamics decreased, the wake density stabilised after 750 s following the cessation of propeller rotation and the position of the laser spot remained constant. The position of the laser spot was stabilised at 0.441 mm, which corresponded to a refractive index change of 3.87×10^{-6} RIU caused by the propeller wake flow field in the detection zone. The laser spot position signal generated by the propeller wake exhibited a decreasing amplitude over time. This phenomenon could be observed as the laser spot displacement gradually diminished as the propeller wake dissipated. Figure 8b illustrates the background position signal, the laser position signal induced by 5 s of propeller rotation, and the laser position signal 25 s after the propeller stops rotating. These signals were measured in the propeller wake for a strongly stratified water environment. The alteration in the laser position signal resulting from the propeller wake was largely in accordance with the simulation outcomes pertaining to the wake field. Figure 8c illustrates the density signal generated by the propeller wake flow, as obtained through CTD measurement. The trend in the density change in the wake field was found to be essentially concordant with the trend in the wake measurement results obtained by means of a PSD-based propeller wake measurement device.
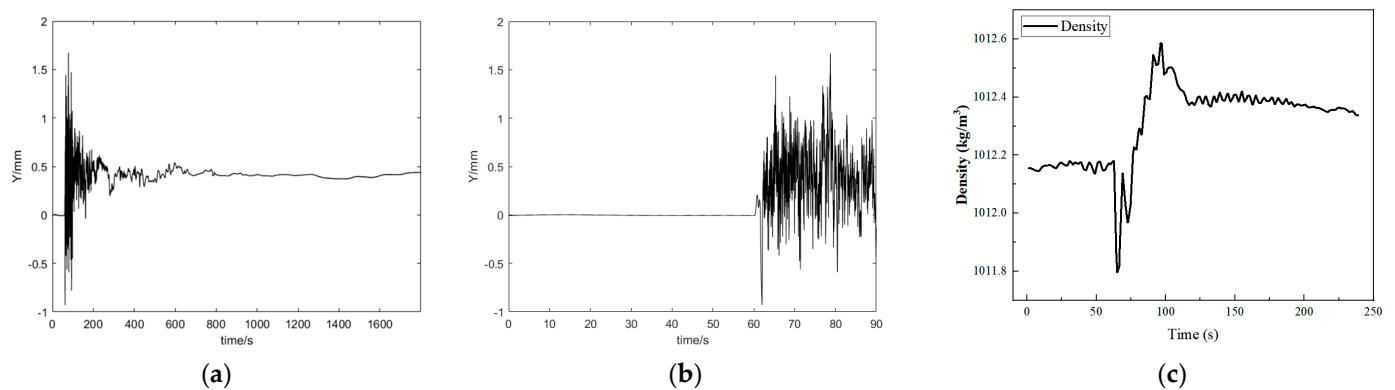
Figure 8. (**a**) The results of propeller wake measurements based on a PSD conducted in a linear density stratification water environment; (**b**) the first 90 s of the results of propeller wake measurements based on a PSD conducted in a linear density stratification water environment; (**c**) the results of propeller wake measurements based on a CTD conducted in a linear density stratification water environment.

5.3. Discussion

Comparing the propeller wake signal characteristics in the two water environments of strong density stratification and linear density stratification, the duration of the propeller wake field dynamics in the case of strong density stratification was about 50 s longer than that in the case of linear density stratification, and the time of drastic change in the laser spot position caused by the propeller wake field was about 120 s longer than that in the case of linear density stratification. The maximum displacement of the laser spot caused by the propeller wake in the case of strong density stratification was larger than that in the case of linear density stratification by 3.016 mm, but the refractive index change in the case of linear density stratification was larger than that in the case of strong density stratification by 8.8×10^{-7} RIU. Therefore, the signal characteristics of the propeller wake field measured using the PSD-based experimental setup of underwater propeller wake measurement were basically the same as those of the simulation results of the propeller wake field. And a comparison of the experimental device-based wake measurements with the CTD-based wake measurements revealed a consistent trend.

In comparison with the existing detection techniques for underwater vehicles, the technique proposed in this paper is capable of detecting refractive index gradient changes of the order of 10^{-9} RIU and is able to detect wake signals after 750 s–800 s of cessation of navigation. In future research, we will refine the parameters of the wake field measurement device to create an in situ detection system, enabling the in situ detection of wake fields of ships and underwater vehicles. Consequently, the positioning and tracking of ships and underwater vehicles can be achieved. The realisation of this detection technique is of great significance for the advancement of research in the field of optical detection of underwater vehicle wake streams.

6. Conclusions

In this paper, we propose a position-sensitive detector-based approach that utilises the laser deflection principle. A theoretical model was developed which describes the relationship between the displacement of a laser spot and the gradient change in the refractive index in the wake field of an underwater vehicle. This model was based on the principle of laser beam deflection. Based on this optical detection method, an experimental apparatus for the detection of the wake current field of underwater vehicles was constructed. Since propellers are the propellers of modern ships and underwater vehicles, propellers were chosen as the power source of the target wake flow. In the design of the experimental setup, a three-bladed propeller with a diameter of 39 mm was selected, the water tank size was 980 mm $\times$ 380 mm $\times$ 380 mm, and the laser acted at a distance of 550 mm from the propeller. The density distribution characteristics of the wake field of the propeller were

simulated and analysed in accordance with the relevant parameters of the experimental apparatus. This was carried out in two cases of strong density stratification and linear density stratification. In order to conduct the experiments and wake field simulations, the propeller was set to rotate at 110 revolutions per second for a period of five seconds, after which it was stopped. The experimental results demonstrate that in a strong density-stratified water environment, the detection signal of the propeller wake field persisted for approximately 800 s. As the wake field power attenuated continuously, the wake field density gradually stabilised, with the final laser spot position stabilising at 0.341 mm. This corresponded to a change in the refractive index of the flow field of 2.99×10^{-6} RIU. In a linear density-stratified water environment, the detection signal of the propeller wake field lasted approximately 750 s. As the wake field power was attenuated continuously, the wake field density gradually stabilised, with the final laser spot position stabilising at 0.441 mm. This corresponded to a change in the refractive index of the flow field of 3.87×10^{-6} RIU. The signal characteristics of the propeller wake field, as measured using the PSD-based experimental setup for underwater propeller wake measurement, were found to be essentially consistent with those of the corresponding simulation results, and the observed trend in experimental device-based wake measurements was consistent with the corresponding trend in CTD-based wake measurements.

In future research, we will refine the parameters of the wake field measurement device to create an in situ detection system, enabling the in situ detection of wake fields of ships and underwater vehicles, and will also facilitate an analysis of the impact of a complex seawater environment on the detection of flow fields. Consequently, the positioning and tracking of ships and underwater vehicles can be achieved.

Author Contributions: Conceptualization, G.Z.; validation, G.Z.; formal analysis, G.Z. and Q.L.; investigation, L.L.; resources, G.Z. and H.W.; writing—original draft, G.Z.; supervision, X.C. and Y.Z.; project administration, L.L.; funding acquisition, Y.Z. All authors have read and agreed to the published version of the manuscript.

Institutional Review Board Statement: Not applicable.

Informed Consent Statement: Not applicable.

Data Availability Statement: Data are contained within the article.

Conflicts of Interest: The authors declare no conflicts of interest.

References

1. Zong, S.G.; Zhang, X.; Duan, Z.K.; Yang, S.P.; Chen, B. Research on Laser Dual-Mode Fusion Detection Method of Ship Wake Bubbles. *Appl. Sci.* **2024**, *14*, 3695. [CrossRef]
2. Higley, P.D. A Low-Cost Acoustic Positioning System for Small Manned Submarines. *IEEE J. Oceanic. Eng.* **1983**, *8*, 113–115. [CrossRef]
3. Kumar, S.; Chinthaginjala, R.; Anbazhagan, R.; Nyangaresi, V.O.; Pau, G. Submarine Acoustic Target Strength Modeling at High-Frequency Asymptotic Scattering. *IEEE Access* **2024**, *12*, 4859–4870. [CrossRef]
4. Kim, H.M.; Hong, S.Y.; Kwon, H.W.; Song, J.H.; Jeon, J.J.; Jung, W.J. Numerical simulation of submarines with anechoic coatings for acoustic target strength reduction. *Nav. Eng. J.* **2012**, *124*, 49–58.
5. Zhou, S.L.; Fang, Z. Optimization Design of Acoustic Performance of Underwater Anechoic Coatings. *Acoust. Aust.* **2022**, *50*, 297–313. [CrossRef]
6. Lan, C.F.; Yu, Z.L.; Chen, H.; Zhang, L.; Zhang, M. Research on Underwater Collaborative Detection Method Based on Complex Marine Environment. *IEEE Access* **2024**, *12*, 3464–3475. [CrossRef]
7. Huang, B.; Liu, Z.Y.; Xu, Y.J.; Ding, Q.C.; Pan, M.C.; Hu, J.F.; Zhang, Q. Characteristics of Magnetic Fields Induced by the Wake of an Underwater Vehicle. *Appl. Sci.* **2022**, *12*, 7964. [CrossRef]
8. Sitefanick, T. The Nonacoustic Detection of Submarines. *Sci. Am.* **1988**, *258*, 41. [CrossRef]
9. Jiang, Y.N.; Yang, Z.Y.; Li, K.; Liu, T. Pre-Processing of Simulated Synthetic Aperture Radar Image Scenes Using Polarimetric Enhancement for Improved Ship Wake Detection. *Remote Sens.* **2024**, *16*, 658. [CrossRef]

10. Tatavarti, R.; Ananth, P.N.; Rajasree, A.K.; Vidyalal, V.; Radhakrishnan, P.; Nampoori, V.P.N.; Vallabhan, C.P.G. Internal Waves-a Novel Measurement Technique. *Curr. Sci.* **1995**, *69*, 678–684.

11. Swain, S.K.; Trinath, K. Non-Acoustic Detection of Moving Submerged Bodies in Ocean. *Int. J. Innov. Res. Dev.* **2012**, *1*, 361–372.

12. Voropayev, S.I.; McEachern, G.B.; Fernando, H.J.S.; Boyer, D.L. Large vortex structures behind a maneuvering body in stratified fluids. *Phys. Fluids* **1999**, *11*, 1682–1684. [CrossRef]

13. Voropayev, S.I.; Smirnov, S.A. Vortex streets generated by a moving momentum source in a stratified fluid. *Phys. Fluids* **2003**, *15*, 618–624. [CrossRef]

14. Bentley, J.P.; Mudd, J.W. Vortex shedding mechanisms in single and dual bluff bodies. *Flow Meas. Instrum.* **2003**, *14*, 23–31. [CrossRef]

15. Schulte-Pelkum, N.; Wieskotten, S.; Hanke, W.; Dehnhardt, G.; Mauck, B. Tracking of biogenic hydrodynamic trails in harbour seals (*Phoca vitulina*). *J. Exp. Biol.* **2007**, *210*, 781–787. [CrossRef]

16. Gläser, N.; Wieskotten, S.; Otter, C.; Dehnhardt, G.; Hanke, W. Hydrodynamic trail following in a California sea lion (*Zalophus californianus*). *J. Comp. Physiol. A* **2011**, *197*, 141–151. [CrossRef]

17. Hanke, W.; Wieskotten, S.; Marshall, C.; Dehnhardt, G. Hydrodynamic perception in true seals (Phocidae) and eared seals (Otariidae). *J. Comp. Physiol. A* **2013**, *199*, 421–440. [CrossRef] [PubMed]

18. Dehnhardt, G.; Mauck, B.; Bleckmann, H. Seal whiskers detect water movements. *Nature* **1998**, *394*, 235–236. [CrossRef]

19. Eberhardt, W.C.; Wakefield, B.F.; Murphy, C.T.; Casey, C.; Shakhsheer, Y.; Calhoun, B.H.; Reichmuth, C. Development of an artificial sensor for hydrodynamic detection inspired by a seal's whisker array. *Bioinspir. Biomim.* **2016**, *11*, 056011. [CrossRef] [PubMed]

20. Dalziel, S.B.; Hughes, G.O.; Sutherland, B.R. Whole-field density measurements by 'synthetic schlieren'. *Exp. Fluids* **2000**, *28*, 322–335. [CrossRef]

21. Elsinga, G.E.; van Oudheusden, B.W.; Scarano, F.; Watt, D.W. Assessment and application of quantitative schlieren methods: Calibrated color schlieren and background oriented schlieren. *Exp. Fluids* **2004**, *36*, 309–325. [CrossRef]

22. Hargather, M.J.; Settles, G.S. A comparison of three quantitative schlieren techniques. *Opt. Laser Eng.* **2012**, *50*, 8–17. [CrossRef]

23. Ben-Gida, H.; Liberzon, A.; Gurka, R. A stratified wake of a hydrofoil accelerating from rest. *Exp. Therm. Fluid Sci.* **2016**, *70*, 366–380. [CrossRef]

24. Stella, A.; Guj, G.; Di Felice, F. Propeller wake flowfield analysis by means of LDV phase sampling techniques. *Exp. Fluids* **2000**, *28*, 1–10. [CrossRef]

25. Paik, B.G.; Ahn, J.W.; Seol, H.S.; Park, Y.H.; Kim, K.; Cheon, H.G. Development of LDV (Laser Doppler Velocimetry) for Measuring Three Dimensional Hull Wake of Ship Model in Large Cavitation Tunnel. *J. Soc. Nav. Archit. Korea* **2017**, *54*, 515–521. [CrossRef]

26. Tatavarti, R.; Sanjaya, K.S.; Trinath, K.; Arulmozhivarman, P. Evolution of Non Acoustic Detection Systems. *Inst. Def. Sci. Technol. J.* **2013**, *12*, 1–13.

27. Zhang, S.W.; Li, L.Y.; Liu, Y.L.; Zhou, Y. Drift Error Compensation Algorithm for Heterodyne Optical Seawater Refractive Index Monitoring of Unstable Signals. *Sensors* **2023**, *23*, 8460. [CrossRef] [PubMed]

28. Wang, L.Z.; Guo, C.Y.; Su, Y.M.; Wu, T.C. A numerical study on the correlation between the evolution of propeller trailing vortex wake and skew of propellers. *Int. J. Nav. Arch. Ocean* **2018**, *10*, 212–224. [CrossRef]

29. Wang, L.Z.; Guo, C.Y.; Xu, P.; Su, Y.M. Analysis of the performance of an oscillating propeller in cavitating flow. *Ocean Eng.* **2018**, *164*, 23–39. [CrossRef]

30. Wang, L.Z.; Guo, C.Y.; Xu, P.; Su, Y.M. Analysis of the wake dynamics of a propeller operating before a rudder. *Ocean Eng.* **2019**, *188*, 106250. [CrossRef]